



# **Mixed-Mode Fracture Analysis of Brittle Intermetallic Compound in Solder Joint**

by

**Ooi Eang Pang  
(1441411349)**

A thesis submitted in fulfillment of the requirements for the degree of  
Doctor of Philosophy

**School of Mechatronic Engineering  
UNIVERSITI MALAYSIA PERLIS**

2019

**DECLARATION OF THESIS AND COPYRIGHT**

Author's Full Name : OOI EANG PANG  
 Date of Birth : 05 AUGUST 1971  
 Title : MIXED-MODE FRACTURE ANALYSIS OF BRITTLE INTERMETALLIC COMPOUND IN SOLDER JOINT  
 Academic Session : 2018/2019

I hereby declare that this thesis becomes the property of Universiti Malaysia Perlis (UniMAP) and to be placed at the library of UniMAP. This thesis is classified as:

- CONFIDENTIAL** (Contains confidential information under the Official Secret Act 1972)\*
- RESTRICTED** (Contains restricted information as specified by the organization where research was done)\*
- OPEN ACCESS** I agree that my thesis to be made immediately available as hard copy or online open access (full text)

I, the author, give permission to reproduce this thesis in whole or in part for the purpose of research or academic exchange only (except during the period of FOUR years, if so requested above). All material contained within the thesis, including without limitation text, logos, icons, photographs and all other artwork, is copyright material of Universiti Malaysia Perlis unless otherwise stated. Use may be made of any material contained within the thesis for non-commercial purposes from the copyright holder. Commercial use of material may only be made with the express, prior, written permission of Universiti Malaysia Perlis.

Certified by:

**SIGNATURE**

710805025253

**(NEW IC NO. /PASSPORT NO.)**

Date: 28 May 2019

**SIGNATURE OF SUPERVISOR**

ASSOC. PROF. IR. DR. RUSLIZAM  
BIN DAUD

**NAME OF SUPERVISOR**

Date: 28 May 2019

## ACKNOWLEDGMENT

First of all, I would like to convey my greatest appreciation to my family whose giving me the strength and fully support in dealing with this research. My greatest gratitude goes to my supervisor Assoc. Prof. Ir. Dr. Ruslizam bin Daud for his encouragement and inspiration on this study. His guidance taught me to be independent and enthusiasm on completing my research project. His support is so great that not only given toward my research but also encompass my well-being as a PhD student.

Special thanks to my co-supervisor Ir. Dr. Nasrul Amri Bin Mohd Amin who provide the technical help in proceeding the research. I extend my thanks to Kementrian Pendidikan Tinggi (KPT) for support in financial and MyPhD scholarship as well.

I would also like to thank my fellow colleagues, postgraduate students and members of Damage and Fracture Mechanics SIG.

Lastly but not least, my most sincere thanks to those have contribute into this project or indirectly toward my well-being whether directly or indirectly during completing this thesis, all other lecturers, all my friends and Unimap's staffs for their helpful advice.

## TABLE OF CONTENTS

|  | <b>PAGE</b>   |
|--|---------------|
| <b>DECLARATION OF THESIS AND COPYRIGHT</b>                           | <b>i</b>      |
| <b>ACKNOWLEDGMENT</b>  | <b>ii</b>     |
| <b>TABLE OF CONTENTS</b>   | <b>iii</b>    |
| <b>LIST OF TABLES</b>  | <b>ix</b>     |
| <b>LIST OF FIGURES</b>   | <b>xv</b>     |
| <b>LIST OF ABBREVIATIONS</b>   | <b>xxviii</b> |
| <b>LIST OF SYMBOLS</b>   | <b>xxix</b>   |
| <b>ABSTRAK</b>   | <b>xxx</b>    |
| <b>ABSTRACT</b>  | <b>xxxi</b>   |
| <b>CHAPTER 1 INTRODUCTION</b>  | <b>1</b>      |
| 1.1 Research Background  | 1             |
| 1.2 Research Motivation  | 5             |
| 1.3 Problem Statements   | 6             |
| 1.4 Research Objective   | 7             |
| 1.5 Research Scope   | 7             |
| 1.6 Thesis Organization  | 8             |
| <b>CHAPTER 2 LITERATURE REVIEW</b>                                   | <b>9</b>      |
| 2.1 Overview of solder joint problems in electronic industries       | 9             |
| 2.2 Solder joint test in industries: ball shear and reliability test | 11            |
| 2.3 Fracture mechanism in solder joint                               | 12            |

|   |   |           |
|---|---|-----------|
| 2.3.1                                   | Formation and growth of IMC layer   | 12        |
| 2.3.2                                   | Effect of thermal aging on secondary IMC layer ( $\text{Cu}_3\text{Sn}$ ) fracture growth | 14        |
| 2.3.3                                   | Void formation affected by grain boundary size of copper                                  | 17        |
| 2.3.4                                   | Void form by electro-migration and current density  | 18        |
| 2.3.5                                   | Creep   | 20        |
| 2.3.6                                   | Effect of introducing trace alloying elements   | 21        |
| 2.4                                     | Solder joint fracture analysis  | 21        |
| 2.4.1                                   | Energy release rate ( $G$ ) analysis approach   | 23        |
| 2.4.2                                   | J-integral ( $J$ ) analysis approach  | 24        |
| 2.4.3                                   | Stress intensity factor (SIF, $K$ ) use in fracture analysis                              | 25        |
| 2.4.4                                   | Multiple cracks interaction based on Kachanov theory                                      | 28        |
| 2.5                                     | Solder joint failure and reliability issues   | 37        |
| 2.5.1                                   | Simulation on the effect of mechanical stress & geometry                                  | 42        |
| 2.5.2                                   | Simulation on material type effect  | 50        |
| 2.5.3                                   | Simulation in ball shear speed test or strain rate factor                                 | 50        |
| 2.5.4                                   | Simulation on reliability test  | 52        |
| 2.6                                     | Experimental work on solder joint fracture analysis                                       | 53        |
| 2.6.1                                   | Experiments on mechanical stress & geometry effect  | 53        |
| 2.6.2                                   | Experimental work on material type related fracture studies                               | 53        |
| 2.6.3                                   | Summary of electrical stress related experiments  | 56        |
| 2.7                                     | Critical review of past studies in the solder joint failure                               | 58        |
| 2.8                                     | Present issue of solder joint   | 61        |
| 2.9                                     | Chapter Summary   | 68        |
| <b>CHAPTER 3 – RESEARCH METHODOLOGY</b> |   | <b>69</b> |
| 3.1                                     | Overview  | 69        |

|       |   |     |
|-------|---|-----|
| 3.2   | Research Design, Methodology and Flow Chart   | 70  |
| 3.3   | Material properties and meshing scheme  | 72  |
| 3.3.1 | Material Properties   | 72  |
| 3.3.2 | Element Type  | 72  |
| 3.3.3 | Global meshing using 8-node quadrilateral element   | 73  |
| 3.3.4 | Singularity & Wedge   | 73  |
| 3.4   | Fracture parameter based on DEM and J-integral  | 75  |
| 3.4.1 | Computation of SIF Using Displacement Extrapolation   | 75  |
| 3.4.2 | Computation of SIF Using J-integral (CINT)  | 78  |
| 3.5   | Convergence meshing and theoretical validation  | 82  |
| 3.6   | Modeling of single edge crack IMC layer   | 87  |
| 3.6.1 | FE Modeling based on ASTM E399-90 (Srawley) Analytical Model  | 87  |
| 3.6.2 | FE Modeling Based on Brown & Srawley Analytical Model   | 88  |
| 3.6.3 | IMC model based on ASTM E399-90 (Srawley) Model   | 89  |
| 3.6.4 | IMC model based on single crack to study the behaviour of solder joint  | 91  |
| 3.7   | Modeling of multiple crack IMC layer based on DEM and CINT  | 94  |
| 3.7.1 | Parallel edge cracks analysis on solder joint behavior  | 94  |
| 3.7.2 | The effect of crack location near interface of solder-IMC   | 97  |
| 3.7.3 | Co-planar cracks Analysis on solder joint behavior  | 99  |
| 3.7.4 | The effect of crack location at solder bulk towards the interface of solder-IMC for two coplanar cracks                     | 103 |
| 3.7.5 | The effect of crack location of two coplanar cracks at IMC layer from copper-IMC interface towards the IMC-solder interface | 105 |
| 3.7.6 | The effect of mixed-mode at IMC for amplification and shielding   | 106 |
| 3.8   | Chapter Summary   | 109 |

|   |            |
|---|------------|
| <b>CHAPTER 4 – RESULT AND DISCUSSION</b>  | <b>110</b> |
| 4.1 Chapter Overview  | 110        |
| 4.2 IMC Geometrical Effect and Singularity Element Refinement   | 111        |
| 4.2.1 Width refinement of IMC model   | 111        |
| 4.2.2 Effect of Height Refinement of IMC Model  | 114        |
| 4.2.3 Singularity Meshing Refinement based on Srawley Equation  | 122        |
| 4.3 Singularity Meshing Refinement based on Brown & Srawley Equation  | 125        |
| 4.3.1 Meshing size refinement   | 126        |
| 4.4 Comparison Between Brown & Srawley and Srawley Model  | 128        |
| 4.4.1 Stress strain behavior  | 130        |
| 4.4.2 Full Numerical Modeling using ASTM E399-90 (Srawley) Equation   | 131        |
| 4.4.3 Validation of Tensile and Shear Test Data   | 134        |
| 4.4.4 Energy Release During Tensile and Shear Loading   | 137        |
| 4.5 Fracture Behavior of Intermetallic Compound (IMC) of Solder Joints Based on Finite Elements Simulation Result | 140        |
| 4.5.1 The effect on different crack length on fracture parameter  | 140        |
| 4.5.2 The effect on different solder thickness on fracture parameter  | 142        |
| 4.5.3 The effect on different IMC thickness on fracture parameter   | 143        |
| 4.5.4 The effect on different Young's Modulus on fracture parameter   | 145        |
| 4.6 Multiple Crack Analysis based on DEM and CINT approach – for Parallel Cracks                                  | 147        |
| 4.6.1 Verification of current FE Model with Analytical reference solution   | 147        |
| 4.6.2 The effect of crack length between 2 parallel edge cracks in Solder Material                                | 148        |
| 4.6.3 The effect of distance (B) between 2 parallel edge cracks   | 150        |

|       |  |            |
|-------|--|------------|
| 4.6.4 | The effect of crack location near solder-IMC's interface of two parallel edge cracks   | 158        |
| 4.7   | Multiple Crack Analysis based on DEM and CINT approach – Co-planar Cracks  | 164        |
| 4.7.1 | The effect of horizontal (x) distance between the coplanar crack tips  | 165        |
| 4.7.2 | The effect of vertical (y) distance between the coplanar crack tips  | 171        |
| 4.7.3 | The effect of coplanar (inner crack) crack length  | 173        |
| 4.7.4 | The effect of crack location of two coplanar cracks from one IMC-solder interface across solder layer towards another solder-IMC interface | 178        |
| 4.7.5 | The effect of crack location of two coplanar cracks across IMC layer from Copper/IMC interface to IMC/solder interface                     | 183        |
| 4.8   | The mix-mode effect of parallel crack and coplanar crack   | 192        |
| 4.8.1 | The impact of horizontal distance between coplanar tip to mix-mode multiple cracks interaction   | 192        |
| 4.8.2 | The impact of vertical distance (y) between parallel crack tips to mix-mode multiple cracks interaction                                    | 196        |
| 4.8.3 | The impact of crack length of crack tip D to mix-mode multiple cracks interaction  | 201        |
| 4.8.4 | The impact of crack length of BC crack line to mix-mode multiple cracks interaction  | 208        |
| 4.9   | Chapter Summary  | 212        |
|       | <b>CHAPTER 5 – CONCLUSION &amp; RECOMMENDATION</b>   | <b>213</b> |
| 5.1   | Chapter Overview   | 213        |
| 5.2   | Conclusion   | 213        |
| 5.3   | Contributions of the research work   | 216        |
| 5.3.1 | Theoretical contribution   | 216        |

|       |  |            |
|-------|--|------------|
| 5.3.2 | Application to solder joints failure assessment      | 217        |
| 5.3.3 | Knowledge contribution to microelectronic industries | 217        |
| 5.4   | Recommendation for Future Work                       | 218        |
|       | <b>REFERENCES</b>                                    | <b>219</b> |
|       | <b>APPENDIX A</b>                                    | <b>227</b> |
|       | <b>APPENDIX B</b>                                    | <b>233</b> |
|       | <b>APPENDIX C</b>                                    | <b>242</b> |
|       | <b>APPENDIX D</b>                                    | <b>254</b> |
|       | <b>APPENDIX E</b>                                    | <b>265</b> |
|       | <b>LIST OF PUBLICATIONS</b>                          | <b>279</b> |

@This item is protected by original copyright

## LIST OF TABLES

|           |   | PAGE |
|-----------|---|------|
| Table 2.1 | A review of stress interaction based on Kachanov's theory   | 35   |
| Table 2.2 | Studies conducted by researchers in solder joint fracture toughness   | 37   |
| Table 2.3 | Summary of geometry factors that affect the behaviour of solder joint (I)   | 47   |
| Table 2.4 | Summary of geometry factors that affect the behaviour of solder joint (II)  | 49   |
| Table 2.5 | Summary of ball shear effect to the fracture toughness of solder joints   | 51   |
| Table 2.6 | Summary of material related fracture studies, their effect and applications   | 55   |
| Table 2.7 | Summary electrical stress related solder joints fracture studies their effect and applications  | 57   |
| Table 3.1 | Properties of materials, Amalu & Ekere (2012)   | 72   |
| Table 3.2 | The relationship between radius of first row element (DELR) on the normalized $K_I/K_{BS}$ for crack length, $a/W = 0.2$ to $0.6$ by DEM  | 82   |
| Table 3.3 | The relationship between radius of first row element (DELR) on the normalized $K_I/K_{BS}$ for crack length, $a/W = 0.2$ to $0.6$ by CINT | 83   |

|            |   |    |
|------------|---|----|
| Table 3.4  | The effect of number of wedge (NTHET) around the crack tip on the ratio $K_I/K_{BS}$ for normalized crack length, $a/W = 0.1$ to $0.6$ using DEM  | 84 |
| Table 3.5  | The effect of number of wedge (NTHET) around the crack tip on the ratio $K_I/K_{BS}$ for normalized crack length, $a/W = 0.1$ to $0.6$ using CINT | 85 |
| Table 3.6  | Refinement dimension obtained from Srawley equation modeling process  | 88 |
| Table 3.7  | Optimum dimension from Brown & Srawley equation modeling process  | 89 |
| Table 3.8  | Dimension for IMC, SAC and Cu   | 89 |
| Table 3.9  | Optimum dimension of FE model for crack length effect study   | 92 |
| Table 3.10 | Optimum dimension of FE model for solder thickness study  | 92 |
| Table 3.11 | Optimum dimension of FE model for IMC thickness study   | 93 |
| Table 3.12 | Optimum dimension of FE model for Young's Modulus study   | 93 |
| Table 3.13 | Optimum dimension for investigating the effect of parallel (stack) cracks location  | 95 |
| Table 3.14 | Optimum dimension of FE model for ratio of parallel edge crack length study   | 96 |
| Table 3.15 | Optimum dimension of FE model to investigate the effect of vertically distance between the two parallel cracks edge                               | 97 |
| Table 3.16 | Optimum dimension for investigating the effect of parallel (stack) cracks location  | 98 |

|            |  |     |
|------------|--|-----|
| Table 3.17 | Optimum dimension of FE model to investigate the effect of two co-planar cracks location at solder material  | 100 |
| Table 3.18 | Optimum dimension of FE model to study the effect of horizontal distance (x) between two co-planar crack tips  | 101 |
| Table 3.19 | Optimum dimension of FE model to study the effect of vertical distance (y) between two co-planar crack tips  | 102 |
| Table 3.20 | Optimum dimension for co-planar FE model to study the effect of inner crack length A2  | 103 |
| Table 3.21 | Optimum dimension of FE model to investigate the effect of two co-planar cracks location at solder material  | 104 |
| Table 3.22 | Optimum dimension for co-planar cracks FE model to study the effect of two co-planar cracks location at IMC layer  | 105 |
| Table 3.23 | Optimum dimension for stack crack and coplanar cracks FE model to study the effect of horizontal distance (x) between tip A and B on the mixed-mode of amplification and shielding | 107 |
| Table 3.24 | Optimum dimension for stack crack and coplanar cracks FE model to study the effect of vertical distance (y) between tip A and D on the mixed-mode of amplification and shielding   | 108 |
| Table 3.25 | Optimum dimension for stack crack and coplanar cracks FE model to study the effect of crack length tip D (A3) on the mixed-mode of amplification and shielding                     | 108 |
| Table 3.26 | Optimum dimension for stack crack and coplanar cracks FE model to study the effect of crack length tip B & C (A2) on the mixed-mode of amplification and shielding                 | 109 |
| Table 4.1  | 1st stage of width determination for width $W = 2.0$ mm, height $\ell = 1.29$ mm   | 112 |

|            |   |     |
|------------|---|-----|
| Table 4.2  | Width effect for $W = 2.2$ mm, $\ell = 1.64$ mm                     | 112 |
| Table 4.3  | 3rd stage of width determination for $W = 2.1$ mm, $\ell = 1.47$ mm | 113 |
| Table 4.4  | Height refinement for $W = 2.1$ mm, $\ell = 1.30$ mm                | 115 |
| Table 4.5  | Height refinement for $W = 2.1$ mm, $\ell = 1.40$ mm                | 115 |
| Table 4.6  | Height refinement for $W = 2.1$ mm, $\ell = 1.50$ mm                | 116 |
| Table 4.7  | Height refinement for $W = 2.1$ mm, $\ell = 1.60$ mm                | 116 |
| Table 4.8  | Height refinement for $W = 2.1$ mm, $\ell = 1.70$ mm                | 117 |
| Table 4.9  | Height refinement for $W = 2.1$ mm, $\ell = 1.45$ mm                | 119 |
| Table 4.10 | Height refinement for $W = 2.1$ mm, $\ell = 1.46$ mm                | 119 |
| Table 4.11 | Height refinement for $W = 2.1$ mm, $\ell = 1.48$ mm                | 120 |
| Table 4.12 | Height refinement for $W = 2.1$ mm, $\ell = 1.49$ mm                | 120 |
| Table 4.13 | Refinement obtained from Srawley modelling process                  | 121 |
| Table 4.14 | Meshing size of 1/10  | 122 |
| Table 4.15 | Meshing size of 1/20  | 123 |
| Table 4.16 | Meshing size of 1/30  | 123 |
| Table 4.17 | Meshing size of 1/50  | 123 |
| Table 4.18 | FE model SIF and C model for $W = 1.0$ mm, $\ell = 1.50$ mm         | 125 |
| Table 4.19 | FE model SIF and C model for $W = 2.0$ mm, $\ell = 3.0$ mm          | 126 |
| Table 4.20 | For meshing size = 1/10, $W = 1.0$ mm, $\ell = 1.50$ mm             | 127 |
| Table 4.21 | For meshing size = 1/20, $W = 1.0$ mm, $\ell = 1.50$ mm             | 127 |

|            |  |     |
|------------|--|-----|
| Table 4.22 | Comparison of Factor C of modeling to Brown & Srawley and Factor $Y_2$ of modeling to standard ASTM E399-90 (Srawley)          | 129 |
| Table 4.23 | The computed SIF when load with difference tensile stress  | 132 |
| Table 4.24 | The computed SIF when load with difference shear stress  | 133 |
| Table 4.25 | The computed SIF (MPa $\sqrt{m}$ ) when load with difference tensile stress  | 135 |
| Table 4.26 | The computed SIF (MPa $\sqrt{m}$ ) when load with difference shear stress  | 136 |
| Table 4.27 | Energy release rate ( $G$ ) calculated from SIF for tensile stress   | 137 |
| Table 4.28 | Energy release rate ( $G$ ) calculated from SIF for shear stress   | 139 |
| Table 4.29 | Normalized SIF of two parallel cracks of equal crack length under normal loading   | 147 |
| Table 4.30 | SIF of parallel crack tips A1 and A2 for varying crack length ratio of A2/A1 (based on DEM)                                    | 149 |
| Table 4.31 | Comparison between difference ratio of crack length on shielding effect  | 157 |
| Table 4.32 | The comparison between present research, Kachanov and Sih analytical solution for coplanar interaction (Qing & Yang, 2006)     | 164 |
| Table 4.33 | SIF change with x-distance between two coplanar crack-tip A & B for vertical distance (y) at 0.0015 mm                         | 165 |
| Table 4.34 | The relationship between SIF at crack-tips A, B, C and the gap between the crack edge towards solder/IMC interface             | 179 |
| Table 4.35 | Relationship between SIF of coplanar crack-tips and their location from solder/IMC, IMC/copper and inside IMC and solder layer | 184 |

|            |   |     |
|------------|---|-----|
| Table 4.36 | Relationship between SIF of coplanar crack-tips and their location from copper/IMC interface across IMC layer to IMC/solder interface | 187 |
| Table 4.37 | The relationship between parallel and coplanar cracks distance and its effect   | 192 |

@This item is protected by original copyright

## LIST OF FIGURES

|            | <b>PAGE</b>  |    |
|------------|--|----|
| Figure 1.1 | SEM images of cross-sectioned mixed solder bump “A” under $1 \times 10^4 \text{ A.cm}^{-2}$ at $100 \text{ }^\circ\text{C}$ for (a) 0 h, (b) 96 h, (c) 180 h. Electromigration failure induced by current crowding (Tian et al., 2013)   | 2  |
| Figure 1.2 | SEM micrograph of the cross sectioned Cu/Sn/Cu joints; (a) as received, (b) after current stressing for 29 h, and (c) after current stressing for 192 h (An et al., 2015)  | 2  |
| Figure 1.3 | The mechanisms of voids formation. (a) before current stressing, (b) growth of $\text{Cu}_6\text{Sn}_5$ , (c) voids formation in the Cu/Sn/Cu joint, and (d) before current stressing, (e) small voids formation, (f) voids condensation in the Cu/IMCs/Cu joint (An et al., 2015) | 3  |
| Figure 2.1 | A schematic drawing showing: (a) flip-chip solder joints, (b) solder joint formation and failure, and (c) formation of barrier layer after addition of elements (X). (Kotadia et al., 2014)  | 13 |
| Figure 2.2 | SEM images of cross-sectional joints with different reflow times at $240 \text{ }^\circ\text{C}$ . (a)25, (b) 120, (c) 240, (d) 480, (e) 720, (f) 960 (min) (Hang et al., 2013)  | 15 |
| Figure 2.3 | SEM images of cross-sectional joints with different reflow times at $300 \text{ }^\circ\text{C}$ . (a)25, (b) 120, (c) 240, (d) 480, (e) 720, (f) 960 (min) (Hang et al., 2013)  | 15 |
| Figure 2.4 | Schematic demonstration of the $\text{Cu}_3\text{Sn}$ -controlling thermal degradation mechanism (Yang et al., 2016)   | 17 |

|             |   |    |
|-------------|---|----|
| Figure 2.5  | The effect of grain size of Cu on the void formation at the interface of Cu <sub>3</sub> Sn/Cu. (a) Small grain size of Cu, and (b) large grain size of Cu. (Li et al., 2015) | 18 |
| Figure 2.6  | (a) The pancake and cotton type voids in the solder joints under electromigration, (b) Voids development under electromigration at 40 h (Wang et al., 2017a)                  | 20 |
| Figure 2.7  | Arbitrary contour around the crack tip of a crack. (Anderson (2005)   | 24 |
| Figure 2.8  | Definition of the coordinate axis ahead of a crack tip. The z direction is normal to the page (Anderson, 2005)  | 25 |
| Figure 2.9  | Singularity elements around the crack tip (Jen et al., 2011)  | 28 |
| Figure 2.10 | (a) Superposition for two cracks; (b) traction on a crack as a sum of its average and a non-uniformity with a zero average (Kachanov M. & Montagut E., 1986)                  | 29 |
| Figure 2.11 | Superposition for two parallel cracks (Kachanov M., 1993)   | 32 |
| Figure 2.12 | The traction on a crack as a sum of its average and a non-uniformity with a zero average (Kachanov M., 1993)  | 33 |
| Figure 2.13 | Model of IMC crack at the IMC-solder interface of shear butt-joint solder sample (Alam et al., 2009a)   | 44 |
| Figure 2.14 | Voids nucleate from the current crowding spot and propagated through the interfaces of solder (Alam et al., 2007a)  | 62 |
| Figure 2.15 | Cracks at the interface of the SnAgCu BGA solder joint on the Au/Ni/Cu metallization during high temperature aging (Alam et al., 2006b)                                       | 63 |
| Figure 2.16 | Kirkendall void formed during aging at 150 °C for 100 hours (Kotadia et al., 2014)  | 65 |

|             |   |    |
|-------------|---|----|
| Figure 2.17 | SEM images of cross-sectional aged solder joints at Stage III. (a – c) 200 $\mu\text{m}$ and (d – f) 600 $\mu\text{m}$ . (Tian et al., 2011)  | 67 |
| Figure 2.18 | (a) and (b) Detailed crack propagation behaviour in Figure 2.17(d) (Tian et al., 2011)  | 67 |
| Figure 2.19 | Microstructures in the interfacial regions of as-reflowed and aged solder joints at Stage III. (a) 200 $\mu\text{m}$ as-reflowed solder joint, (b) 600 $\mu\text{m}$ solder joint as-reflowed solder joint, (c) 200 $\mu\text{m}$ aged solder joint for 36 days, (d) 600 $\mu\text{m}$ aged solder joint for 36 days. (Tian et al., 2011) | 68 |
| Figure 3.1  | Research Flow Chart   | 71 |
| Figure 3.2  | Geometry of PLANE 183   | 73 |
| Figure 3.3  | (a) Singular elements in PLANE 183 (b) 8-nodes singularity element  | 74 |
| Figure 3.4  | DEM method to determine SIFs by picking the node in the crack tip and face  | 77 |
| Figure 3.5  | The output result for KCALC command for SIF $K_I$ , $K_{II}$ & $K_{III}$  | 78 |
| Figure 3.6  | Output result of CINT command to compute the SIF, $K_I$   | 81 |
| Figure 3.7  | The effect of the radius of first row element (DELR) on SIF by DEM  | 82 |
| Figure 3.8  | The effect of the radius of first row element (DELR) on SIF by CINT   | 83 |
| Figure 3.9  | The effect of number of wedge (NTHET) around the crack tip on the normalized $K_I/K_{BS}$ for normalized crack length, $a/W = 0.1$ to $0.6$ using DEM   | 85 |
| Figure 3.10 | The effect of number of wedge (NTHET) around the crack tip on the normalized $K_I/K_{BS}$ for normalized crack length, $a/W = 0.1$ to $0.6$ using CINT  | 86 |

|             |  |     |
|-------------|--|-----|
| Figure 3.11 | Meshing for ASTM E399-90 Srawley Model   | 88  |
| Figure 3.12 | Meshing for Brown & Srawley Model  | 89  |
| Figure 3.13 | (a) Model for a crack at IMC interface of solder joint b) Model in tensile stress c) Model in shear stress condition   | 90  |
| Figure 3.14 | The FE Model validated with Brown & Srawley analytical equation for shorter edge crack studies   | 94  |
| Figure 3.15 | The FE Model validated with Kachanov (1989) analytical solution for two equal size of parallel cracks  | 95  |
| Figure 3.16 | The FE Model validated with Brown & Srawley analytical equation for two parallel crack length studies  | 96  |
| Figure 3.17 | The FE Model validated with Brown & Srawley analytical equation for two parallel edge crack tips location studies  | 98  |
| Figure 3.18 | (a) FE model used to validate with Kachanov teory (b) Two colinear crack with the same length used by Qing, H. & Yang, W. (2006) in validation with Sih's and Kachanov's analytical solution | 99  |
| Figure 3.19 | The FE Model validated with Brown & Srawley Analytical equation for two co-planar crack tips studies   | 101 |
| Figure 3.20 | Geometry of FE for coplanar cracks interaction in solder bulk region   | 104 |
| Figure 3.21 | The FE model geometry for co-planar cracks interaction in IMC layer for varying vertical distance from copper-IMC interface  | 105 |
| Figure 3.22 | FE geometry for mixed-mode of amplification and shielding in IMC layer   | 107 |
| Figure 4.1  | Shape correction factor for 1 <sup>st</sup> refinement   | 111 |

|             |   |     |
|-------------|---|-----|
| Figure 4.2  | Shape correction factor for 2 <sup>nd</sup> refinement  | 113 |
| Figure 4.3  | Shape correction factor for 3 <sup>rd</sup> refinement  | 114 |
| Figure 4.4  | $Y_2$ factors of difference height of 2.1 mm width FE models are plotted against crack length per width                   | 118 |
| Figure 4.5  | Zoom in of graphs in Fig. 4.4 for $a/W$ range 0.45 to 0.70  | 118 |
| Figure 4.6  | $Y_2$ factors of 1.45 to 1.49 mm height of 2.1 mm width IMC models are plotted against crack length per width             | 121 |
| Figure 4.7  | Graphs of difference meshing are plotted against crack length per width   | 124 |
| Figure 4.8  | Comparison between SIF computed from Brown & Srawley equation and ANSYS modeling  | 128 |
| Figure 4.9  | Comparison between $Y_2$ & $C$ constant of theoretical equation and ANSYS numerical modeling                              | 129 |
| Figure 4.10 | von Mises contour stress analysis show the maximum stress is located at the edge of IMC layer of full model without crack | 130 |
| Figure 4.11 | Zoom out on the crack tip at the IMC layer of the full model under tensile loading  | 131 |
| Figure 4.12 | The relationship between $K_I$ , $K_{II}$ with the tensile stress   | 132 |
| Figure 4.13 | Zoom out on the crack tip at the IMC layer of the full model under shear loading  | 133 |
| Figure 4.14 | The relationship between $K_I$ , $K_{II}$ with the shear stress   | 134 |
| Figure 4.15 | The relationship between $K_I$ , $K_{II}$ (MPa $\sqrt{m}$ ) with the tensile stress                                       | 135 |
| Figure 4.16 | Graph of the relationship between $K_I$ , $K_{II}$ (MPa $\sqrt{m}$ ) with the shear stress                                | 136 |

|             |  |     |
|-------------|--|-----|
| Figure 4.17 | Energy release rate during tensile loading   | 138 |
| Figure 4.18 | Energy release rate during shear loading   | 139 |
| Figure 4.19 | Stress intensity factor $K_I$ obtained when difference shear stress applied on varying crack length  | 140 |
| Figure 4.20 | Stress intensity factor $K_{II}$ obtained when difference shear stress applied on varying crack length   | 141 |
| Figure 4.21 | SIF affected by difference shear stress for difference solder thickness  | 142 |
| Figure 4.22 | The influence of solder thickness on fracture parameter (stress intensity factor $K_I$ ) at difference shear stress                                  | 143 |
| Figure 4.23 | The effect of difference IMC thickness on stress intensity factor $K_I$ for varying shear stress   | 144 |
| Figure 4.24 | The effect of difference Young's Modulus on stress intensity factor $K_I$ for varying shear stress   | 146 |
| Figure 4.25 | von Mises stress distribution for crack tip Young's modulus 43 GPa and 110 GPa respectively under shear stress of 12 MPa and crack length of 0.05 mm | 146 |
| Figure 4.26 | SIF of parallel crack-tips against normalized crack length $A_2/A_1$   | 149 |
| Figure 4.27 | SIF at $A_1$ & $A_2$ crack tips against distance between the two parallel cracks with crack length ratio of $A_2:A_1 = 0.3$                          | 150 |
| Figure 4.28 | Normalized SIF at $A_1$ & $A_2$ crack tips against distance between the two parallel cracks with crack length ratio of $A_2:A_1 = 0.3$               | 151 |
| Figure 4.29 | Stress intensity factor at $A_1$ & $A_2$ crack tips against distance between the two parallel cracks with crack length ratio of $A_2:A_1 = 1.0$      | 152 |

|                |   |     |
|----------------|---|-----|
| Figure 4.30    | Normalized stress intensity factor at A1 & A2 crack tips against distance between the two parallel cracks with crack length ratio of A2:A1 = 1.0                  | 152 |
| Figure 4.31    | Stress intensity factor at A1 & A2 crack tips against distance between the two parallel cracks with crack length ratio of A2:A1 = 1.5                             | 154 |
| Figure 4.32    | Normalized stress intensity factor at A1 & A2 crack tips against distance between the two parallel cracks with crack length ratio of A2:A1 = 1.5                  | 155 |
| Figure 4.33    | Stress at A1 & A2 crack tips against distance between the two parallel cracks with crack length ratio of A2:A1 = 2.0  | 155 |
| Figure 4.34(a) | Normalized SIF at A1 & A2 crack tips against distance between the two parallel cracks with crack length ratio of A2:A1 = 2.0                                      | 156 |
| Figure 4.34(b) | Summary for all normalized SIF at A1 & A2 crack tips against distance between the two parallel cracks with crack length ratio of A2:A1 = 0.3, 1.0, 1.5 & 2.0      | 157 |
| Figure 4.35    | Stress intensity factor of A2/A1 at A1 & A2 crack tips against distance between the two parallel cracks with crack length ratio of A2:A1 = 0.1, 0.3, 0.5 and 0.8  | 158 |
| Figure 4.36    | Stress intensity factor (SIF) of crack-tip A1 and A2 against their distance from Solder-IMC interface in solder layer for 0.004 mm (B) between the two crack-tips | 159 |
| Figure 4.37    | Normalized stress intensity factor (SIF) of crack-tip A1 and A2 against their distance from Solder-IMC interface for 0.004 mm (B) between the two crack-tips      | 159 |

|             |  |     |
|-------------|--|-----|
| Figure 4.38 | Stress of crack-tip A1 and A2 against their distance from Solder-IMC interface for 0.050 mm (B) between the two crack-tips         | 160 |
| Figure 4.39 | Normalized SIF of crack-tip A1 and A2 against their distance from Solder-IMC interface for 0.050 mm (B) between the two crack-tips | 160 |
| Figure 4.40 | Stress of crack-tip A1 and A2 against their distance from Solder-IMC interface for 0.080 mm (B) between the two crack-tips         | 161 |
| Figure 4.41 | Normalized SIF of crack-tip A1 and A2 against their distance from Solder-IMC interface for 0.080 mm (B) between the two crack-tips | 161 |
| Figure 4.42 | Stress of crack-tip A1 and A2 against their distance from Solder-IMC interface for 0.150 mm (B) between the two crack-tips         | 162 |
| Figure 4.43 | Normalized SIF of crack-tip A1 and A2 against their distance from Solder-IMC interface for 0.150 mm (B) between the two crack-tips | 162 |
| Figure 4.44 | SIF against horizontal-distance (x) between two coplanar crack-tips for vertical distance (y) at 0.0015 mm                         | 166 |
| Figure 4.45 | Normalized SIF against horizontal-distance (x) between two coplanar crack-tips for vertical distance (y) at 0.0015 mm              | 166 |
| Figure 4.46 | SIF against horizontal distance (x) between two coplanar crack-tips for vertical distance (y) at 0.0026 mm                         | 167 |
| Figure 4.47 | Normalized SIF against horizontal distance (x) between two coplanar crack-tips for vertical distance (y) at 0.0026 mm              | 167 |
| Figure 4.48 | SIF against x-distance between two coplanar crack-tips for vertical distance (y) at 0.005 mm                                       | 168 |

|             |   |     |
|-------------|---|-----|
| Figure 4.49 | Normalized SIF against x-distance between two coplanar crack-tips for vertical distance (y) at 0.005 mm                               | 168 |
| Figure 4.50 | SIF against x-distance between two coplanar crack-tips for vertical distance (y) at 0.010 mm  | 169 |
| Figure 4.51 | Normalized SIF against x-distance between two coplanar crack-tips for vertical distance (y) at 0.010 mm                               | 169 |
| Figure 4.52 | SIF versus vertical distance (y) between two coplanar crack-tip for horizontal distance (x) 0.0010 mm                                 | 172 |
| Figure 4.53 | Normalized SIF versus vertical distance (y) between two coplanar crack-tip for horizontal distance (x) 0.0010 mm                      | 172 |
| Figure 4.54 | Stress intensity factor against inner crack length A2 of crack-tips B & C for x = 0.00102 mm and y = 0.0015 mm                        | 176 |
| Figure 4.55 | Normalized stress intensity factor against inner crack length A2 of crack-tips B & C for x = 0.00102 mm and y = 0.0015 mm             | 176 |
| Figure 4.56 | Stress intensity factor against inner crack length A2 of crack-tips B & C for x = 0.050 mm and y = 0.050 mm                           | 177 |
| Figure 4.57 | Normalized stress intensity factor against inner crack length A2 of crack-tips B & C for x = 0.050 mm and y = 0.050 mm                | 177 |
| Figure 4.58 | SIF at the coplanar crack-tips versus the distance between the crack edge and solder/IMC interface in solder layer                    | 179 |
| Figure 4.59 | Normalized SIF of $KE$ at the coplanar crack-tips versus the distance between the crack edge and solder/IMC interface in solder layer | 180 |
| Figure 4.60 | Normalized SIF at the coplanar crack-tips versus the distance between the crack edge and solder/IMC interface in solder layer         | 180 |

|             |  |     |
|-------------|--|-----|
| Figure 4.61 | (a) The two coplanar cracks at 0.010 mm from the solder/IMC interface (b) von-Mises stress of the two coplanar cracks at 0.010 mm from the solder/IMC interface  | 183 |
| Figure 4.62 | SIF of coplanar crack-tips against the distance of edge crack from Copper for 0.001025 mm gap between the two coplanar crack-tips  | 184 |
| Figure 4.63 | Normalized SIF of coplanar crack-tips against the distance of edge crack from Copper for 0.001025 mm gap between the two coplanar crack-tips (x)   | 185 |
| Figure 4.64 | SIF of coplanar crack-tips against the distance of edge crack from Copper for 0.00305 mm gap between the two coplanar crack-tips   | 188 |
| Figure 4.65 | Stress intensity factors profile across Cu/IMC interface, IMC layer, IMC/solder interface and solder bulk in micro-scale   | 189 |
| Figure 4.66 | Normalized stress intensity factors profile across Cu/IMC interface, IMC layer, IMC/solder interface and solder bulk in micro-scale  | 190 |
| Figure 4.67 | Stress intensity factors profile across Cu/IMC interface, IMC layer, IMC/solder interface and solder bulk in large scale for horizontal x distance between the crack tip A and B of 0.001025 mm            | 191 |
| Figure 4.68 | Normalized stress intensity factors profile across Cu/IMC interface, IMC layer, IMC/solder interface and solder bulk in large scale for horizontal x distance between the crack tip A and B of 0.001025 mm | 191 |
| Figure 4.69 | The mix-mode of amplification and shielding when both parallel and coplanar cracks are near to each other  | 193 |

|             |  |     |
|-------------|--|-----|
| Figure 4.70 | Normalized SIF on the mix-mode of amplification and shielding when both parallel and coplanar cracks are near to each other  | 193 |
| Figure 4.71 | (a) Normalized $K_E$ of crack tip B (b) Normalized SIF $K_E$ of crack tip A, C and D against vertical distance between tip A and D   | 196 |
| Figure 4.72 | von Mises stress when distance between tip A and D ( $y$ ) is (a) 0.003 mm (b) 0.005 mm, (c) 0.007 mm and (d) 0.008 mm   | 197 |
| Figure 4.73 | SIF of crack tip A against vertical distance between tip A and D   | 197 |
| Figure 4.74 | SIF of crack tip B against vertical distance between tip A and D   | 198 |
| Figure 4.75 | SIF of crack tip C against vertical distance between tip A and D   | 198 |
| Figure 4.76 | SIF of crack tip D against vertical distance between tip A and D   | 199 |
| Figure 4.77 | The impact of crack length D on stress amplification and shielding   | 201 |
| Figure 4.78 | The relationship between normalized SIF ( $K_E/K_{EO}$ ) with varying crack length D on stress amplification and shielding   | 202 |
| Figure 4.79 | (a) Meshing and element stress of crack tip A, B and D when crack length of crack tip A and D are the same (b) von Mises stress showing amplification exist among crack tip A, B and D | 204 |
| Figure 4.80 | (a) Meshing and element stress of crack tip A, B and D when crack length of crack tip D right above crack tip B (b) von Mises stress showing amplification only exist among crack tip  |     |

|             |   |     |
|-------------|---|-----|
|             | B and D while tip A does not have any amplification effect with tip B   | 205 |
| Figure 4.81 | (a) Meshing and element stress of crack tip A, B and D when crack length of crack tip D above crack line BC after leaving crack tip B (b) von Mises stress showing amplification still exist between crack tip B and D while tip A does not have any amplification effect with tip B    | 205 |
| Figure 4.82 | (a) Meshing and element stress of crack tip A, B and D when crack length of crack tip D parallel with and at the middle above crack line BC (b) von Mises stress showing no amplification effect exist among crack tip A, B and D but tip C become amplify                              | 205 |
| Figure 4.83 | (a) Meshing and element stress of crack tip A, B and D when crack length of crack tip D right above crack tip C (b) von Mises stress showing amplification only exist among crack tip C and D while tip A & B do not have any amplification effect with tip B                           | 206 |
| Figure 4.84 | The impact of crack length tip A on stress amplification and shielding  | 206 |
| Figure 4.85 | The relationship between normalized SIF ( $K_E/K_{EO}$ ) with varying crack length tip A on stress amplification and shielding  | 207 |
| Figure 4.86 | (a) Meshing and element stress of crack tip A, B and D when crack length of crack tip A below crack line BC after leaving crack tip B (b) von Mises stress showing amplification exist between crack tip A and B which were 2.4 and 1.8 respectively when crack length tip A = 0.017 mm | 207 |
| Figure 4.87 | (a) von Mises stress showing no amplification effect exist among crack tip A, B and D but tip C become amplify when   |     |

crack length tip A = 0.0235 mm (b) von Mises stress showing no amplification effect exist among crack tip A, B and D but tip C become amplify when crack length tip A = 0.0265 mm 208

Figure 4.88 (a) von Mises stress showing amplification exist among crack tip A and C when crack length of crack tip A right below crack tip C (b) von Mises stress showing no amplification exist between crack tip A and C when crack length tip A = 0.041 mm and tip A bear most stress 208

Figure 4.89 Effective SIF of crack tip A, B, C and D change with varying crack length of BC crack line 209

Figure 4.90 Normalized SIF ( $K_E/K_{EO}$ ) against crack length of BC crack line 209

Figure 4.91 von Mises stress of crack tip A, B, C and D when crack length of crack tip B and C is (a) 0.005 mm (b) 0.025 mm (c) 0.080 mm and (d) 0.120 mm 211

@This item is protected by original copyright

## LIST OF ABBREVIATIONS

|        |  |
|--------|--|
| ATC    | Accelerated thermally cycled                 |
| APDL   | Ansys Parameter Design Language              |
| ASTM   | American Standard of Testing and Measurement |
| BGA    | Ball grid array                              |
| CED    | Crack energy density                         |
| CTOD   | Crack tip opening displacement               |
| CZM    | Cohesive Zone Model                          |
| DELR   | Radius of first row element                  |
| DEM    | Displacement Extrapolation Method            |
| EBSD   | Electron backscatter diffraction             |
| ED CCL | Electrodeposited Copper Clad Laminate        |
| EDX    | Energy-dispersive X-ray                      |
| EPFM   | Elastic Plastic Fracture Mechanics           |
| FE     | Finite Element                               |
| FEA    | Finite Element Analysis                      |
| HTOL   | High temperature operating life              |
| HTST   | High thermal shock test                      |
| LTOL   | Low temperature operating life               |
| LEFM   | Linear Elastic Fracture Mechanics            |
| IMC    | Intermetallic compound                       |
| NTHET  | Number of wedges around the crack tip        |
| PCB    | Printed circuit board                        |
| PLM    | Polarized light microscopy                   |
| SAC    | Lead-free tin-silver-copper SnAgCu           |
| SEM    | Scanning Electron Microscopy                 |
| SERR   | Strain energy release rate                   |
| SMT    | Surface mount technology                     |
| SVGGM  | Statistical void growth model                |
| UCP    | Unified creep plasticity                     |

## LIST OF SYMBOLS

|                |  |
|----------------|--|
| $a$            | Crack length                                     |
| $a/W$          | Crack-to-width ratio                             |
| $Cu$           | Copper   |
| $E$            | Young's modulus                                  |
| $G$            | Strain energy release rate                       |
| $J$            | $J$ contour integral approach                    |
| $J_{el}$       | $J$ -elastic                                     |
| $J_{pl}$       | $J$ -plastic                                     |
| $K_{IBS}$      | Stress intensity factor mode I Brown and Srawley |
| $K_{IS}$       | Stress intensity factor mode I Srawley           |
| $SnPb$         | Tin-lead   |
| $\nu$          | Poisson's ratio                                  |
| $\sigma$       | Tensile stress                                   |
| $\sigma_{max}$ | Maximum von Mises                                |
| $\sigma_{ij}$  | Stress tensor                                    |
| $f_{ij}$       | Dimensionless function of $\theta$               |
| $\mu$          | Shear modulus                                    |

@This item is protected by original copyright

## Analisa Patah Mod Campuran Sebatian Intermetalik Rapuh Sambungan Pateri

### ABSTRAK

Lapisan sebatian intermetalik (IMC) yang terbentuk di antara bahan pateri dan kuprum merupakan kawasan patah yang paling lazim berlaku dalam sambungan pateri bergantung kepada jenis and mod pembebanan. Berdasarkan kes kegagalan sambungan pateri dalam industri, bebanan mekanik mencetuskan corak patah mod campuran di mana pertumbuhan retakan-mikro bermula di lapisan IMC. Perlakuan patah IMC yang kompleks kini tidak dapat diterangkan dengan teori untuk menentukan tegasan perlindungan dan penguatan. Kajian ini bertujuan untuk menilai kelakuan patah IMC sambungan pateri berdasarkan teori interaksi Kachanov. Pada permulaan, dua model elemen unsur terhingga (FE) dibina sebagai asas IMC sambungan pateri untuk menentukan dimensi tepat bagi lebar dan panjang lapisan IMC yang disahkan dengan model Srawley dan Brown & Srawley. Kemudian, model IMC retakan-mikro sisi tunggal dimasukkan ke dalam model lengkap pateri sambungan, satu siri analisa tegasan von-Mises dilakukan untuk menentukan kawasan penumpuan tegasan yang kritikal sebelum parameter patah seperti faktor keamatan tegasan (SIF) dan kadar perlepasan tenaga terikan (SERR) dinilai. Dalam pembentukan model IMC, algorithm FE dibina dengan perisian ANSYS APDL untuk membentuk satu model FE bagi kegagalan lapisan IMC sambungan pateri berdasarkan Kaedah Ekstrapolasi Penyesaran (DEM) dan J-integral. Merujuk kepada kelakuan patah model Brown & Srawley dan Srawley, model baru IMC sambungan pateri terus disimulasikan sifat retakan-retakan mikro yang berselari dan segaris yang berbeza bagi menilai tegasan perlindungan dan penguatan secara individual dan bertindih dalam bebanan ricih dan tegangan. Penjelasan interaksi elastik retakan-retakan mikro dirujuk kepada teori interaksi retakan Kachanov, model Brown & Srawley dan Srawley. Keputusan simulasi menunjukkan bahawa bahan pateri menjadi kurang kuat jika retakan yang lebih panjang wujud dalam sambungan itu. Lapisan IMC yang lebih tebal dapat mengurangkan sedikit faktor tegasan SIF pada hujung retakan manakala penukaran bahan pateri kepada lapisan IMC akan mengurangkan kekuatan patah sambungan pateri. Interaksi di antara banyak retakan sisi pada bebola pateri dijalankan untuk mengira kesan perlindungan dan pembesaran pada daya pandu retakan berdasarkan kaedah singulariti tegasan dan SERR. Retakan makro didapati membekalkan perlindungan ke atas retakan yang lebih kecil atau retakan-mikro. Jarak di antara dua retakan sisi berselari yang lebih besar akan mengurangkan kesan perlindungan. Apabila dua retakan segaris semakin dekat, tegasan mengalami peningkatan dan menunjukkan kesan penguatan. Selain itu, kesan panjang retakan dalaman dan jarak menegak dikemukakan. Didapati bahawa apabila membandingkan kedua-dua kesan perlindungan dan penguatan, jarak di antara dua hujung retakan mesti kecil untuk memberi interaksi yang berkesan. Lokasi banyak retakan termasuk kedua-dua bahan pateri dan lapisan IMC telah dibincangkan. Ia juga mendedahkan bahawa kedua-dua kaedah menjadi tak stabil apabila kedua-dua hujung retakan saling mendekati. Kesan mod-campuran perlindungan dan penguatan di antara retakan berselari dan segaris memaparkan bahawa keamatan penguatan menjadi dominan jika lebih banyak hujung retakan disusun dalam bentuk segaris manakala keamatan perlindungan menjadi lebih besar apabila konfigurasi semua hujung retakan yang berhampiran adalah dalam mod berselari. Lebih banyak simulasi perlu dijalankan pada masa depan untuk memahami kesan bentuk dan orientasi retakan-retakan yang berbeza di bawah bebanan statik dan dinamik.

## Mixed-Mode Fracture Analysis of Brittle Intermetallic Compound in Solder Joint

### ABSTRACT

Intermetallic compound (IMC) layer formed between solder materials and copper is typically the fracture sites for most of the solder joints subjected to type and mode of loading. Based on industrial failure case of solder joints, mechanical loading has resulted with mixed mode fracture pattern which the micro cracks growth initiated at the IMC layer. The complex fracture IMC behaviour is presently unexplained by theory to define the individual and overlapping stress shielding and stress amplification of micro cracks. This study aims to investigate the fracture behaviour of IMC solder joint based on Kachanov theory of interaction. Initially, two finite element (FE) models were developed for IMC solder joint to find the fit width and length value of the IMC layer, which validated with Brown & Srawley and Srawley model. Then, the single edge micro crack IMC model is embedded into full solder joint model, a series of von-Mises stress analysis is conducted to identify the critical stress concentration area before the fracture parameter e.g. stress intensity factor (SIF) and strain energy release rate (SERR) are evaluated. In IMC model establishment, FE codes are developed using ANSYS APDL software to execute the FE modelling of solder butt joints IMC layer failure based on displacement extrapolation method (DEM) and J-integral. By reliable agreement of fracture behaviour with Brown & Srawley and Srawley model, the new IMC solder joint model is continued for different parallel and coplanar micro cracks behaviour simulation to evaluate the individual and overlapping stress shielding and stress amplification subjected to shear and tensile loading. The micro cracks interaction is elucidating based on Kachanov theory of crack interaction in relating to Brown & Srawley and Srawley model. The results display that soldering material become less tough if greater crack length is present in the joint. The thicker IMC has slightly reduced the SIF on the crack tip but the change from solder to IMC layer decrease the solder joint fracture toughness. The interaction between multiple edge cracks in solder ball was carried out to quantify the effect of shielding and amplification on the crack driving force based on stress singularity and strain energy release rate approach. Larger length of macro-crack is found to provide shielding to the smaller crack or micro-crack. The greater distance between the two parallel edge cracks will reduce the shielding effect. When two co-linear cracks are closer together, the stress increases and demonstrated the amplification effect. Besides, the effect of inner crack length and vertical distance are highlighted. It is found that when compare both shielding and amplification, the distance between the two crack-tip must be shorter to give better effect. Location of multiple cracks include both soldering bulk and IMC layer were discussed. It also reveals that both approaches become unstable when both crack-tip are near together. The effect of mix-mode shielding and amplification between parallel and co-linear cracks demonstrates that the amplification become dominant if more crack tips are array in co-linear pattern, while shielding is in prevailing when the configuration of the very near crack tips all are in stack mode. More simulation should be carried out in future to understand the effect of difference shape and orientation of cracks under both static and dynamic loading.

## CHAPTER 1 : INTRODUCTION

### 1.1 Research Background

The electronics products failure was related to thermomechanical, electromechanical or chemical corrosion damage and the majority are involved with fracture failure. One of the failures of the product which draws major concern is solder joints failure. Failure analysis of electronic products has accelerated the study of solder joints defect and the way to prevent the failure. Many researches on solder joint fracture study were focused on mechanical, thermal and electric-thermal stress (Jen, et al., 2011; Tian et al., 2011; Amalu et al., 2012; Alam et al., 2009a & b; Nadimpalli & Spelt, 2011; Yao et al., 2010). Based on those studies, mechanical stress, temperature cycle, thermal shock, operating life cycle and environment test are the most significant test to ensure the reliability and lifetime of the electronic devices.

Solder joint failure mostly related to the fracture at the intermetallic compounds (IMC) layer which attracted major further detail studies. The formation, growth of IMC was notified to trigger nucleation of microcrack and micro-void, and then propagate and coalesce to cause a fracture in the joint. The evolution and morphology of intermetallic grains ( $\text{Cu}_6\text{Sn}_5$  and  $\text{Cu}_3\text{Sn}$ ) have been investigated by Tian et al. (2011, 2013, 2014), Liang et al. (2017), Liu et al. (2015), Alam et al. (2007, 2008, 2009) explained the growth of IMC layer induced by thermal ageing and electrical stress. Subsequently, the microvoids and microcracks formed and combine to form a larger void or crack.

Furthermore, high electrical stress or high current density also found to be the cause of joint failure due to Joule thermal heating and electromigration. Electromigration of copper atoms at the substrate (pad) by high current density can cause large Kirkendall void (Alam et al., 2007a; Tian et al., 2013; An et al., 2015; Wang et al., 2017a) that lead to catastrophic failure at the joint. Apart from that, a dynamic mechanical impact like loading rate and vibration also affect the reliability of the solder joint (Shen & Aluru, 2010; Qin et al., 2012a). Figure 1.1 shows electromigration failure induced by current crowding in Tian (2013) study. Figure 1.2 reveals the experiment result after being electric stress for different duration of time by An et al. (2015), while Figure 1.3 explained the mechanism of void formation and growth of IMC layer during electric stress carried out by An et al. (2015).

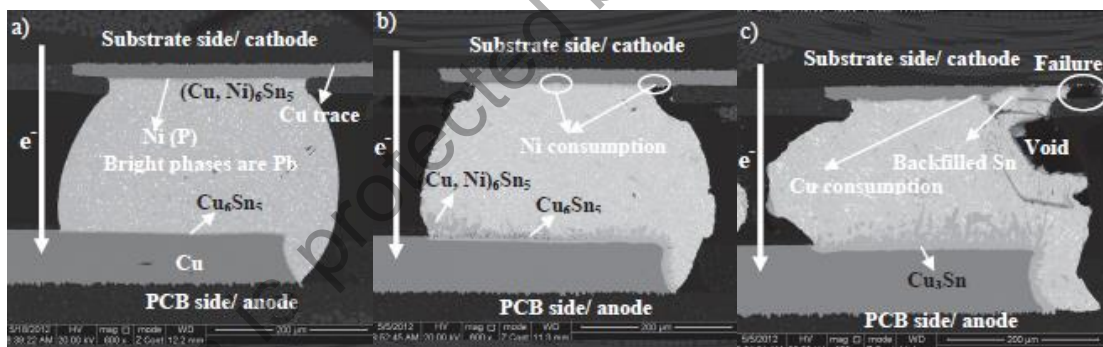


Figure 1.1 SEM images of cross-sectioned mixed solder bump “A” under  $1 \times 10^4 \text{ A.cm}^{-2}$  at  $100^\circ\text{C}$  for (a) 0 h, (b) 96 h, (c) 180 h. Electromigration failure induced by current crowding (Tian et al., 2013)

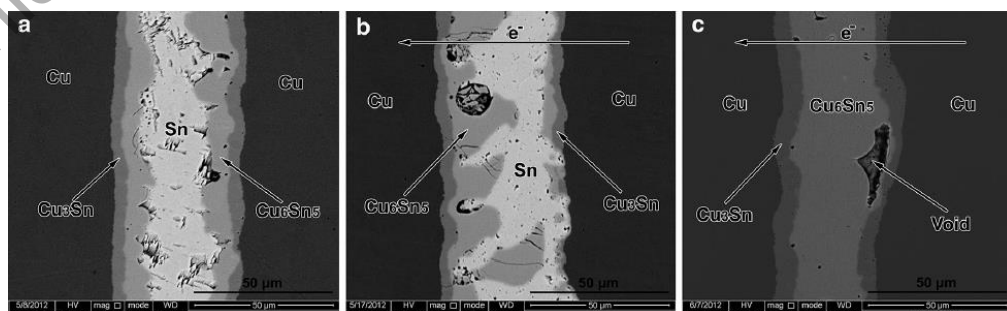


Figure 1.2 SEM micrograph of the cross sectioned Cu/Sn/Cu joints; (a) as received, (b) after current stressing for 29 h, and (c) after current stressing for 192 h (An et al., 2015)

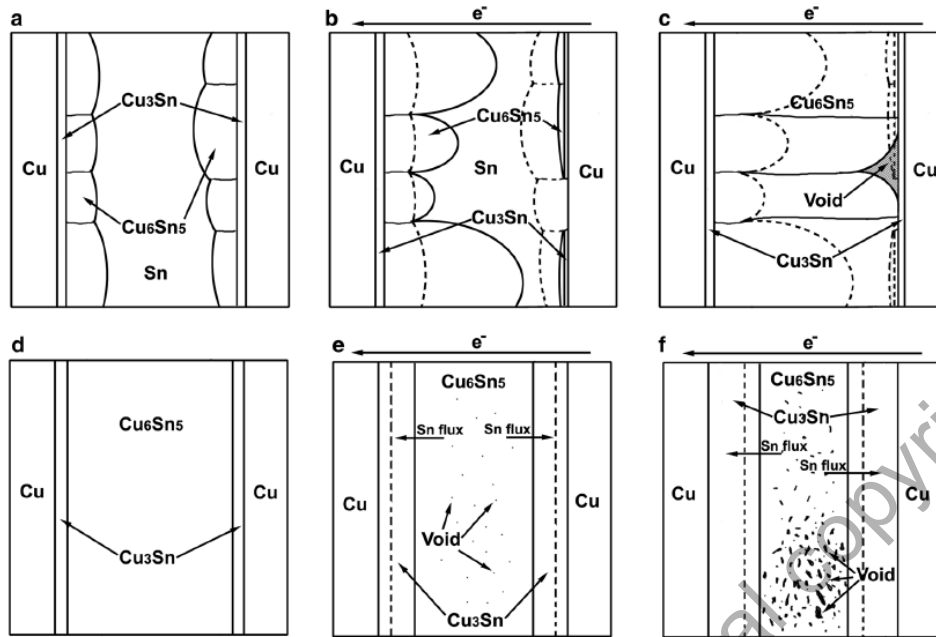


Figure 1.3 The mechanisms of voids formation. (a) before current stressing, (b) growth of  $\text{Cu}_6\text{Sn}_5$ , (c) voids formation in the Cu/Sn/Cu joint, and (d) before current stressing, (e) small voids formation, (f) voids condensation in the Cu/IMCs/Cu joint (An et al., 2015)

The solution to the fracture of the solder joint is mainly focused on the type of additive material that added into the solder material so that it hinders the growth of IMC layer. The material of bond pad also received high interest and many studies have been made using nickel, gold and silver as pad metallization (Alam et al., 2002, 2006a, b, 2008; Chen & Yu et al., 2014). The addition of minor material such as Bi, In, Cu, Zn and Ag to solder material system such as SAC105, SAC305, SAC405 have been carried out intensively to improve their mechanical properties as well as lower its melting temperature. (Ou et al., 2005; Islam et al., 2005; Lejuste et al., 2013; El-Daly et al., 2013; Lee et al., 2001; Kotadia et al., 2014; Prakash & Sritharam, 2004; Yu et al., 2012; Alam et al., 2006; Yao et al., 2010).

In recent years, out of many solder joint failure cases, the problem of interfacial solder joint failure with multiple microcracks were not extensively evaluated by

interacting stress theories (e.g. Kachanov theories). The interfacial layer should be based on IMC layer fracture as a reference before analyse the complete Cu–SAC IMC layer solder joint fracture. To understand the interfacial Cu–SAC IMC layer fracture behaviour, experiment on materials additive and nanoparticles in solder alloy, computer simulation using finite element (FE) analysis method has been employed by many researchers for the fracture analysis of solder joints. By using FE methods, the investigation can be carried out to characterise the fractured joint due to geometry, materials mix-match, thermal stress, type of loading, difference shear rate and electrical stress. The result of the simulation is validated with experiment or theoretical data based on linear elastic fracture mechanic (LEFM) and elastic plastic fracture mechanic (EPFM) approach. Therefore, more investigation on micro-level can be carried out to analyse the behaviour and strength of interfacial Cu–SAC IMC solder joint materials. The result is very useful to predict the failure mode and help in product design development. To date, most of the interfacial Cu–SAC IMC fracture behaviour prediction was based on the single crack analysis and less work is conducted on the multiple cracks analysis. Thus, the assessment parameter may provide inaccurate and unreliable prediction of fracture behaviour for the cases that involved many cracks such as coplanar and parallel cracks in IMC layer. Kachanov's theory of multiple cracks interaction has been applied in this study because Kachanov has developed quite a comprehensive studies on many cracks interaction as a basic reference compare to others such as Sih and Tada (Sih, 1970; Tada et al., 2000).

## 1.2 Research Motivation

The critical solder joint failure sites were reported occurs at brittle IMC layer especially the interface between solder-IMC, numerous data show it fails under brittle intergranular fracture which was due to a combination of many flaws that near-by together. At present, the IMC layer fractures were not used as reference and were not based on any analytical methods which provided theoretical assumption of the governing equations.

In realities, there are many cracks and micro-voids that cause ductile and brittle fractures (Alam et al., 2007a; Tian et al., 2013a & b; Liu, B.L. et al., 2014; Hang, C.J. et al., 2014; Li, H.L. et al., 2015). Presently, interfacial Cu-SAC IMC solder joint failure analysis using simulation has been carried by many researchers to understand the fracture mechanism and help to arrest the cause to prolong the life of the joint and hence increase its reliability towards the products. However, most of the interfacial Cu-SAC IMC simulations were based on a single crack. It is observed that the details multiple cracks interaction effect in interfacial Cu-SAC IMC fracture has been neglected such as mixture of shear & tensile loading, parallels coplanar microcrack orientation, solder joint materials and quantification of stress shielding and amplification to induce crack growth. Thus, the studies of interfacial Cu-SAC IMC solder joint behaviour based on multiple cracks can provide a better explanation to the actual scenario and failure mechanism that exist in most electronics devices during failure. Simulations on multiple cracks have become an important task to give a true picture of fracture behaviour at the solder joint.

### 1.3 Problem statements

Solder joints failure due to excessive electrical stress, thermal and mechanical loads is a significant reliability concern in electronic devices. This has caused complex stress shielding and stress amplification to promote interfacial IMC cracking. From literature (Alam et al., 2009a & b)), it was known that for the sake of simplicity, little attention is paid to the design and development of predicting method to evaluate the fracture behaviour of the interfacial Cu–SAC IMC solder joint which initiated by multiple cracking interaction subjected to mixed-mode loading (Mode I & II). Mechanically, the solder joints especially the IMC layer which has very low critical stress intensity factor,  $K_{IC}$  (1.4-2.85 MPa $\sqrt{m}$ ) compare to solder bulk (70 MPa $\sqrt{m}$ ) that can easily cause the microvoids or micro-cracks nucleation at the IMC-solder interface. These micro-voids or cracks may interact with one another depend on their arrangement. The further study on microcracks interaction will clarify the effect of stress shielding between parallel cracks. This also explains clearly the behaviour of stress amplification that takes effect between two near coplanar crack tips. The combination of parallel and coplanar cracks should reflex the actual multiple cracks interaction between the microcracks in the IMC layer which enable the prediction of fracture load, prevalent fracture mode, exact joint interconnect size and life of interfacial Cu–SAC IMC joints under brittle and fatigue failure.

## 1.4 Research Objectives

This study aims to investigate and evaluate the failure mechanism behaviour of interfacial Cu–SAC IMC layer based on single crack and multiple microcracks interaction. Toward the success of the study, four objectives are formulated for this research as follows:

- (i) To develop and verify the reference numerical IMC layer model based on analytical Brown & Srawley model and ASTM E399-90 Srawley model.
- (ii) To evaluate fracture parameter of single edge microcrack interfacial Cu–SAC IMC model.
- (iii) To evaluate the stress shielding and stress amplification intensity of interfacial Cu–SAC IMC layer cracking subjected to static tensile and shear loading.
- (iv) To evaluate the overlapping mixed mode stress shielding and stress amplification intensity behaviour of interfacial Cu–SAC IMC subjected to static tensile and shear loading.

## 1.5 Research Scope

For the completion of this research, some scopes have been made and state as below:

- (i) This study is limited to the static mechanical loading (tensile and shear stress) of solder joints.
- (ii) The study is based on the linear elastic fracture mechanics (LEFM) applied to the intermetallic compound (IMC) layer and lead-free solder alloy.

- (iii) The experiment simulation is using ANSYS numerical modeling process to analyze the fracture parameter.
- (iv) A two-dimensional (2D) brittle fracture model is used for the study.

## 1.6 Thesis Organization

This thesis consists of five chapters and organized as the following order. Chapter 1 presents the brief of research motivation, related research issues and problem statement, research objective and scopes. Chapter 2 describes the summary of past studies including various failure analysis approaches on the fracture behaviours of the solder joint, experimental works and difference model of simulation to solve various solder joint problems. Lastly, research highlight on the present research gap is addressed.

Chapter 3 presents the detail of the research planning and execution to conduct the numerical simulation works including pre-processing and post-processing works using ANSYS APDL FEA software. This includes the method for sensitivity analysis and verification processes. Chapter 4 outlines the obtained results and discussion based on Kachanov's theory, analytical model results and previous study data for verification and validation. Finally, chapter 5 describes the overall conclusion and summary of the whole research. The achievement and contribution of this research as well as the recommendation future works are listed.

## CHAPTER 2: LITERATURE REVIEW

### 2.1 Overview of solder joint problems in electronic industries

Solder joint materials provide electrical conduction, thermal and mechanical interconnection to joint different components, chips and circuits in electronic assemblies. Solder has been a basic thing in the accomplishment of all electronic products since the beginning of the electronic age, and soldering is anticipated that it will remain the primary assembly and interconnection technology even in the future. Since the functionality and lifetime of an electronic product is directly affect the durability and reliability of solder joints, the solders used must be optimised in terms of their physical and chemical properties to provide tough interconnections. It has long been known that solder joints denote a potential weak point in all electronic products and they will not function if their component joint fail regardless of the highly sophistication of the electronic systems.

The great demand toward miniaturisation form of electronic products led to the smaller size of solder joints. Highly integrated circuit with new technology enable stacking of layers of electronic components interconnected together and the design is composed by different type of materials. The products are designed for higher induced stress levels, tough operating environment and more stringent reliability requirement. In addition, legislation in the European Union and elsewhere has moved to restrict lead use because of the environmental and health concerns associated with it (Kotadia et al., 2014). The phase in of lead-free solders as green environment demand has made the solder joint facing more reliability threat. Tin-lead solder have been used so long because of its

excellent mechanical behaviours like good wetting properties as well as low melting point. Lead is reported as a cheap and non-reactive solvent for tin and it also help reduces the surface tension of tin during wetting (Cheng et al., 2017). The introduction of lead-free solder, especially tin-silver-copper (SnAgCu or SAC) is containing very high percent of tin and requires higher reflow temperature. As a result, solder joint quality and reliability become very critical and one of the major concerns in microelectronic products failure.

The tin lead alloys are used as solder substance while the main substrates are made of copper. The tin in solder will react with copper to form an intermetallic compounds (IMC) which provides good wetting and bonding. However, the growth of thicker layer of IMC became damaging because of its brittleness and tend to cause fracture in the interconnection under low stress (Balakrisnan et al., 2003). Recently, many of the intermetallic compounds (IMCs) were found to grow on the interface between the pad and the solder material (Tian et al., 2011; Balakrisnan et al., 2003). The brittle property of IMCs caused the strong stress concentration effect during the mechanical impacts (Siow & Manoharan, 2005; Lee & Jeong, 2014) and thermal cycles (Jen et al., 2011). The cracks were found to initiate and propagate near the IMC layers. Moreover, the IMC layer grow thicker when the joints are exposed to high temperature during operation and service. Both the internal heat generated by the electronic chips and external heat from the surrounding contribute to the high thermal stress on the joints. The interface between IMC and solder become a site for nucleation of cracks and fracture (Chen et al., 2005; Alam et al., 2009a & b; Qin et al., 2012 a & b; Wang et al., 2012). Therefore, the IMC was considered to have significant effect on the solder joints reliability and the related studies have received great interest in research.

## 2.2 Solder ball shear and reliability test in industries

The functionality of electronic products depends on the solder joint quality which ensure the mechanical strength and stability on the assembly. Thus, the reliability of solder joint is very crucial in the industries. Various tests were introduced to measure the reliability of the joint. Premature failure of the joint is caused by induced stresses due to mismatches in the coefficient of thermal expansion on difference materials in the packages during assembly process like reflow and temperature stress in the operation of the packages. Usually, new design product must be evaluated to establish their reliability and operating life.

Among the common reliability test applied are high temperature operating life (HTOL), high thermal shock test (HTST) (Zhong et al., 2015), low temperature operating life (LTOL), temperature cycle (JEDEC standard: JESD22-A1 04B, 2000), mechanical load cycle, drop impact test, vibration test and humidity stress. The aim of reliability tests is to provide equivalent failure mechanisms which appear during service conditions for the specific product design and produce failure mode effect analysis for the package failures. The failure of solder joints is influenced by some occurrences, like microstructure transformation, creep deformation, stress strain, thermal expansion coefficient of difference materials mix-match, electrical stress, electro-migration, fatigue damage accumulation and dynamic failure. The accelerated test result define the failure life time statistical value for the assembly packages subjected to specific reliability test, whereas the failure analysis result of these packages identifies the main mechanisms of failure (Tamin & Shaffiar, 2014).

Beside reliability test, the most common in-line process test during electronic package assembly is ball shear test and drop shock test to evaluate the strength of solder joint/ball attachment. The typical value of solder ball shear force may range from 30 grams (for 4 mils flip chip solder ball) to more than 1000 grams (for 30 mils ball grid array (BGA)solder ball). The conventional ball shear test method is adopted from the ball shear test of gold wire bonding and in year 2000, JEDEC has established a new standard JESD22-B117 for BGA ball shear test, while JESD22-B111 is the common standard for drop testing (Cheng et al., 2017).

### **2.3 Fracture mechanism in solder joint**

Failure mechanism of solder joint is a process of how a solder joint material and its microstructure change until the interconnection fail. Many studies have been carried out to investigate and identify the mechanism of failure. Among the causes are related to the formation of IMC layer, the growth of IMC layer under thermal stress, the formation of voids which further weaken the IMC layer and propagates of crack.

#### **2.3.1 Formation and growth of IMC layer**

Intermetallic compounds (IMCs) are formed as a result of interaction between solder and metal to form joints in electronic packaging during soldering (Prakash & Sritharan, 2001; Balakrisnan et al.,2003; Wu et al., 2004). Any processing defect or thermomechanical fatigue induces cracks at IMC layer of the solder joint, which will reduce the integrity of the device severely. Therefore, it is essential to understand the

process of the interfacial interactions, formation and growth of IMCs at solder/substrate interfaces. The formation IMC layer consists of several microstructure evolutions, which include nucleation, growth and coarsening. Among these transforming, IMC nucleation is critical because the particular sequence of IMCs formed can greatly influence the morphology and evolution of IMC layers. The IMC growth becomes a problem where an electronics package will experience serious temperature gradients and cyclic mechanical loading through vibration or shock impact (Prakash & Sritharan, 2001; Qin et al., 2012b). The interfacial IMC formation between component/solder/substrate and its failure after aging is shown schematically in Figure 2.1.

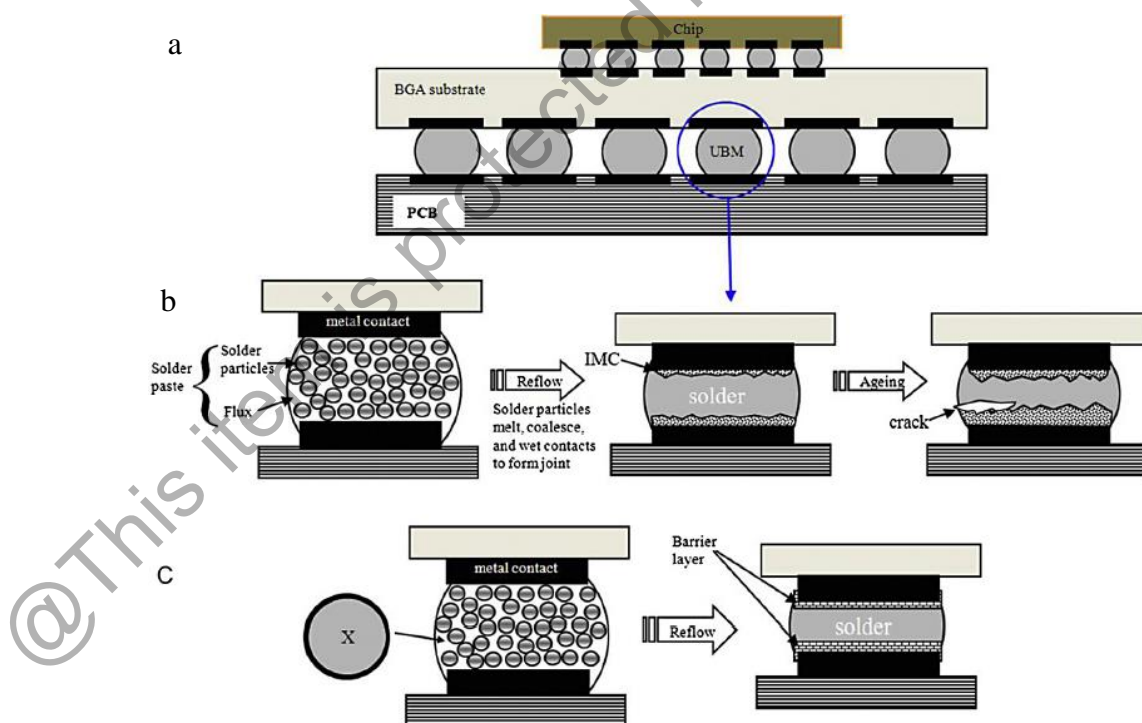


Figure 2.1. A schematic drawing showing: (a) flip-chip solder joints, (b) solder joint formation and failure, and (c) formation of barrier layer after addition of elements (X). (Kotadia et al., 2014)

The most common solution to improve the interfacial reactions and the properties of IMC layers is to alloy the solders with small amounts of additional elements or nanoparticles (Zhang & Tu, 2014). It is noted that the presence of impurities in the interconnection system may also have marked effects on the properties and growth of IMC layers due to their ability to form thin and void-free IMCs at the interface and new interfacial IMC barriers that reduce or prevent the reaction and decrease the growth rate (Kotadia et al., 2014; Cheng et al., 2017).

### **2.3.2 Effect of thermal aging on secondary IMC layer ( $\text{Cu}_3\text{Sn}$ ) fracture growth**

When the SAC solder continues to react with copper (Cu), the  $\text{Cu}_6\text{Sn}_5$  IMC layer becomes thermodynamically unstable on the Cu substrate. As this instability increases, the  $\text{Cu}_3\text{Sn}$  IMC layer begins to form (Balakrisnan et al., 2003; Hang et al., 2013; Tian et al., 2013) by consuming and converting the  $\text{Cu}_6\text{Sn}_5$  IMC layer. During ageing the  $\text{Cu}_3\text{Sn}$  layer grows significantly between the Cu and  $\text{Cu}_6\text{Sn}_5$ , and therefore plays a critical role in determining the reliability of the solder joint. The behaviour of  $\text{Cu}_3\text{Sn}$  during its growth is strongly dependent on the diffusion of the dominant reactive species and on the reaction pathway. Over time, a large amount of voids form in the  $\text{Cu}_3\text{Sn}$  layer, either by the Kirkendall effect or by solute segregation (Li et al., 2015).

Experiment carried out by Hang et al. (2013) revealed that phase conversion of the pure copper-tin IMC layer was gained in copper-tin-copper interfacial. Initially, the  $\text{Cu}_6\text{Sn}_5$  grains was formed and then it continued to grow from both interfacial until they to contact and joint with each other as shown in Figures 2.2-2.3. Consequently, the  $\text{Cu}_3\text{Sn}$

grains formed between the  $\text{Cu}_6\text{Sn}_5$  layer and Cu substrates. The  $\text{Cu}_3\text{Sn}$  grains grew up by converting and consuming the  $\text{Cu}_6\text{Sn}_5$  layer (Zhang et al., 2013b).

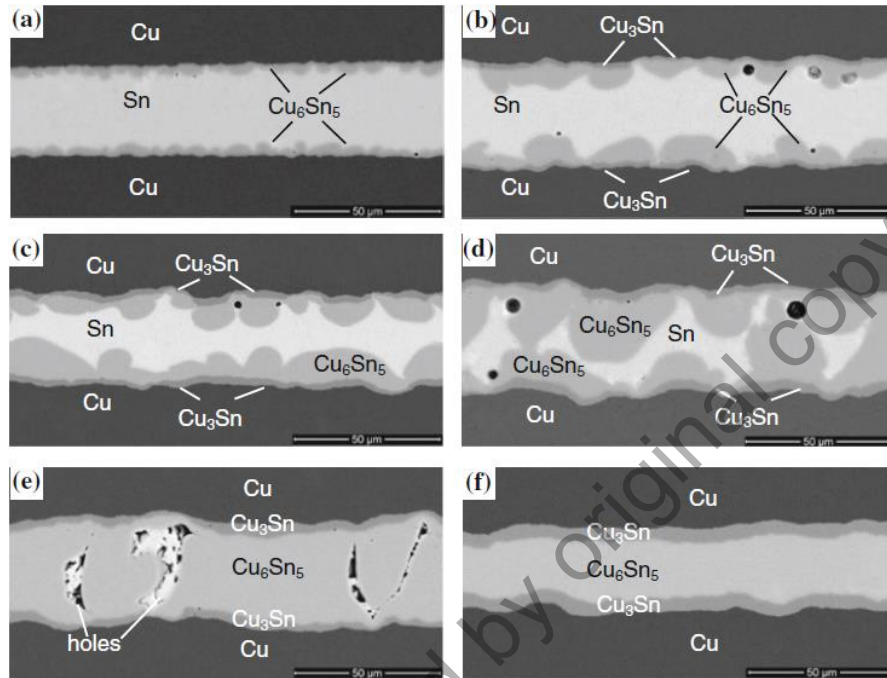


Figure 2.2 SEM images of cross-sectional joints with different reflow times at 240 °C. (a) 25, (b) 120, (c) 240, (d) 480, (e) 720, (f) 960 (min) (Hang et al., 2013)

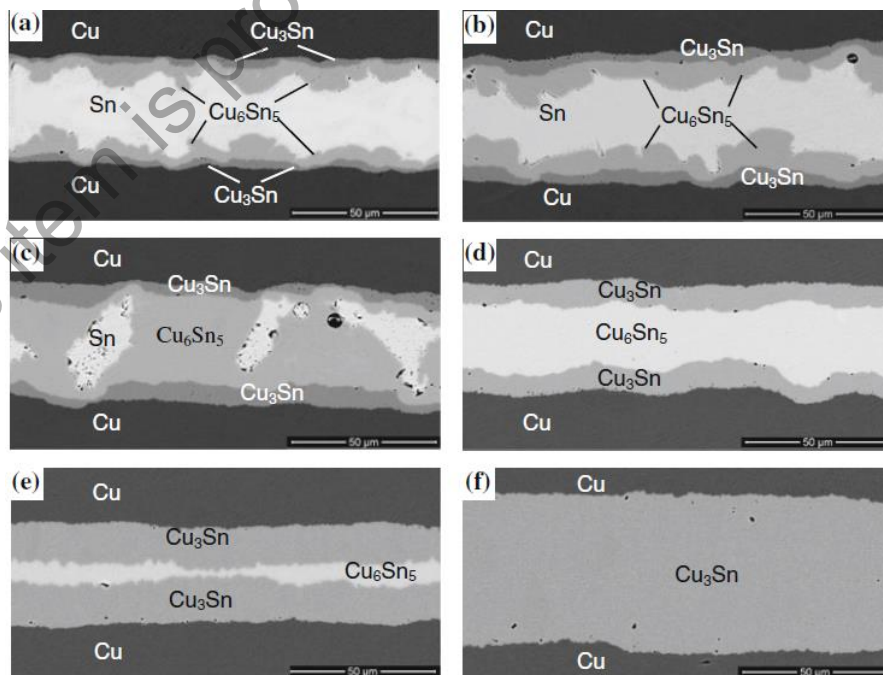


Figure 2.3 SEM images of cross-sectional joints with different reflow times at 300 °C (a) 25, (b) 120, (c) 240, (d) 480, (e) 720, (f) 960 (min) (Hang et al., 2013)

Finally, as shown in the experiment with prolong duration (960 min) at higher temperature (300 °C), only  $\text{Cu}_3\text{Sn}$  IMC phase was found in the solder joint. The same thing was done by Balakrisnan (2001) to prepare Sample  $\text{Cu}_3\text{Sn}$  layer which was annealed at 150 °C to completely establish the  $\text{Cu}_3\text{Sn}$  IMC. Another sample was annealed at a lower temperature of 50 °C to form  $\text{Cu}_6\text{Sn}_5$  and to avoid the conversion of this  $\text{Cu}_6\text{Sn}_5$  phase to  $\text{Cu}_3\text{Sn}$ . Besides Hang et al. (2013), another experiment conducted by Yang et al. (2016) explained the evolution of thermal aging to form IMC  $\text{Cu}_6\text{Sn}_5$  and  $\text{Cu}_3\text{Sn}$  layer. From the study, Yang et al. (2016) found the growth of the  $\text{Cu}_3\text{Sn}$  layer was due to the formation of new  $\text{Cu}_3\text{Sn}$  grains at the triple-junction area along the  $\text{Cu}_3\text{Sn}$ /Copper boundary.

The growth also affected by the angular elongation of the  $\text{Cu}_3\text{Sn}$  grains. Thus, the  $\text{Cu}_3\text{Sn}$  layer was gradually changed from a single-stack structure to a multi-stack structure after a longer aged. There are three failure modes found during high speeds ball pull test: (i) the transgranular cleavage of the  $\text{Cu}_6\text{Sn}_5$  grains, (ii) the interfacial fracture between the  $\text{Cu}_6\text{Sn}_5$  and  $\text{Cu}_3\text{Sn}$  layers and (iii) the  $\text{Cu}_3\text{Sn}$  intergranular fracture. For beginning aging period stage, including the as-reflow condition, only the first two types of fracture mode were observed on the sample. Along with the thermal aging process, the fracture site in the IMC layer gradually moved from the  $\text{Cu}_6\text{Sn}_5$  layer and the  $\text{Cu}_6\text{Sn}_5$ / $\text{Cu}_3\text{Sn}$  interface and eventually to inside the  $\text{Cu}_3\text{Sn}$  layer (Hang et al., 2013; Zhang et al., 2013b). This can be explained from the microstructure evolution of  $\text{Cu}_3\text{Sn}$  layer during the thermal aging. As the  $\text{Cu}_3\text{Sn}$  layer showed an intergranular fracture mode, the fracture actually happens at the  $\text{Cu}_3\text{Sn}$  grain boundary. However, after the soldering process, only a single-stack of  $\text{Cu}_3\text{Sn}$  grains was formed between the  $\text{Cu}_6\text{Sn}_5$  layer and the Cu substrate. When the  $\text{Cu}_3\text{Sn}$  grain boundaries became a joint path, the fracture

would happen in the IMC  $\text{Cu}_3\text{Sn}$  layer and the strength of the whole IMC was reduced. This mechanism is shown in Figure 2.4. Therefore, when the solder joint thermal aging for a longer period such as 1000 h in the study, the intergranular fracture of the  $\text{Cu}_3\text{Sn}$  layer became dominant. Reference to all the finding, microstructure of the  $\text{Cu}_3\text{Sn}$  layer determines the strength of the IMC in the solder joint.

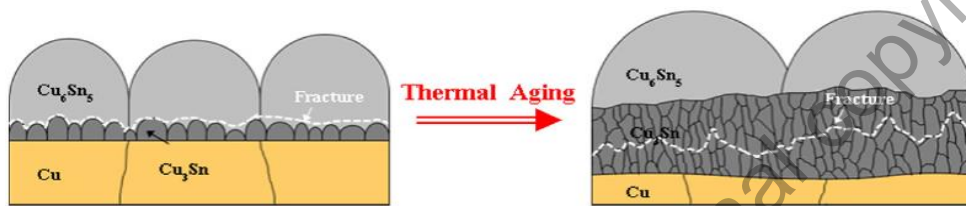


Figure 2.4: Schematic demonstration of the  $\text{Cu}_3\text{Sn}$ -controlling thermal degradation mechanism (Yang et al., 2016)

### 2.3.3 Void formation affected by grain boundary size of copper

Voids formation within the IMC-copper interface was one of the incidences that cause the further propagation of crack and lead to failure in solder joint. A great finding from Li et al. (2015) investigation is grain boundary diffusion, which is one of the most important diffusion mechanisms to explain void formation especially at low temperature. During the solid-state aging, copper is the major diffusion particle. Hence, there should be plenty of vacancies left at or near the interface of IMC  $\text{Cu}_3\text{Sn}$  and copper substrate ( $\text{Cu}_3\text{Sn}/\text{Cu}$ ). It can be inferred that only the vacancies on or near the grain boundaries (GBs) could diffusion easily, while the vacancies inside the grain would be fixed. The vacancies on or near the grain boundaries, which can move freely, could be defined as the effective vacancies (EVs). Only when there are plenty of EVs could the voids form at the interface of  $\text{Cu}_3\text{Sn}/\text{Cu}$ . The smaller the grain size is, the more EVs exist at the interface. If lots of vacancies diffuse into the grain boundaries, the vacancies would get

together and joint up to form voids at the interface, as shown in Figure 2.5(a). That's why lots of voids appeared at the interface of SAC305/ED CCL (Electrodeposited Copper Clad Laminate) with smaller grain size. As for the annealed ED CCL with larger grain size, although there are lots of vacancies, most of them cannot move freely, namely the amount of EVs is small, so they cannot gather to form big voids at the interface, as shown in Figure 2.5(b). For the HPOFC (High Purity Oxygen Free Copper, 99.9999 weight%) plate with bigger grain size than annealed ED CCL, due to fewer EVs, there are no voids formed at the interface.

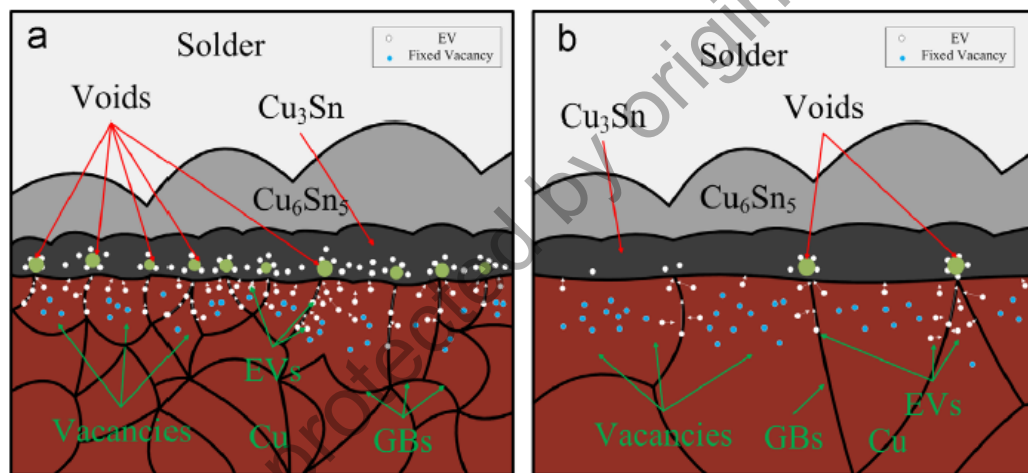


Figure 2.5. The effect of grain size of Cu on the void formation at the interface of  $\text{Cu}_3\text{Sn}/\text{Cu}$ . (a) Small grain size of Cu, and (b) large grain size of Cu. (Li et al., 2015)

#### 2.3.4 Void form by electro-migration and current density

Void also can be formed during high electric stress. From Wang et al. (2017a) study, electromigration is continuous moving of ions in a conductor as a result of the momentum transfer from mobile electrons and the diffusing metal (copper) atoms. This phenomenon usually happened when high current density are applied. With the

decreasing size of microelectronic product, the working current densities are increasing rapidly, and electromigration becomes a serious problem in solder joints. Different from the traditional electromigration issues in the aluminium-copper in integrated circuits interconnects, when electromigration take effect in the solder joints, copper atoms gradually diffuse into solder bulk material which will cause the copper circuit to decline and eventually break the circuit. However, same as ICs interconnects, nucleation, propagation and coalescence of void occur and form a crack in the solder interconnect during high current density application (Alam et al., 2007a; Tian et al., 2013). Compared with the electromigration induced voids in the ICs interconnects, the voids in the solder joints are more complicated. Figure 2.6 shows two types of electromigration induced failure modes in solder joints: cotton or pancake type voids. At the beginning stage, the voids were mainly cotton type, and were distributed randomly in the solder. Under prolong electrical stress, the circular voids would combine into a pancake void and cause interconnect failure. Compared with the pancake type void, more cotton type voids are observed at a lower electrical stress.

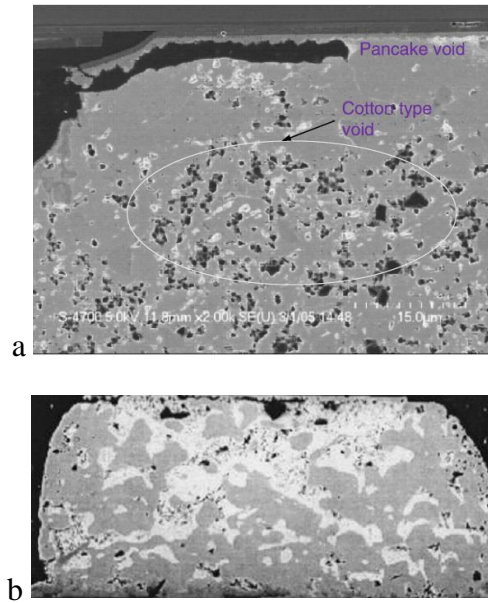


Figure 2.6: (a) The pancake and cotton type voids in the solder joints under electromigration, (b) Voids development under electromigration at 40 h (Wang et al., 2017a)

### 2.3.5 Creep

From the experiment conducted by Zhang & Zhang (2011, 2013a), the results reveal that the thermal fatigue process has two stages: a strain hardening stage and a consequent accelerating fracture stage. Strain hardening of the solder keeps developing at the begin of cycles, until it becomes balance with the dynamic recovery. Microcracks was induced at the corner of the solder joint due to the strain concentration. The damage rate accelerates with increasing cycles. Plastic deformation, grain rotation and grain coalesce occur in the solder during the thermal fatigue process, while grain subdivision or recrystallization was not observed, because the dynamic recovery keeps the strain energy of the solder at a low level. Two main creep deformation mechanism are dislocation climb and grain boundary sliding. Inter-facial plastic deformation of the solder is much more serious at higher strain amplitude, causing lower self-life (Zhang & Tu, 2014).

### **2.3.6 Effect of introducing trace alloying elements**

At the current stage, one of the most usable method to solve the problem in solder joint fracture due to IMC is the addition of trace elements or nanoparticles in order to improve solder joint material properties and reliability. Although this work is not simple and requires much research and development, various alloying elements have been studied, including Ag, Al, Bi, Cd, Cu, In, Sb and Zn (Kotadia et al., 2014; Zhong et al., 2016). All the related work must be with lower melting temperature of the solder alloy because higher temperatures would not suitable for electronics assembly, since most of polymeric materials are with low heat resistance. As the result, five basic systems of tin-copper (Sn-Cu), tin-silver (Sn-Ag), tin-silver-copper (SAC), tin-zinc (Sn-Zn) and tin-bismuth (Sn-Bi) have been introduced as basic lead-free solder system to replace tin-lead solders (Zhang and Tu, 2014). Unfortunately, these high-tin leadfree solder alloy system incur reliability issue including excessive formation of IMC, growth of interfacial IMCs during high temperature storage and occurrence of void. The selectively mixed with trace elements mainly to control the IMC thickness, slow its growth, modify its morphology, prevent disruptive phase changes and increase toughness (Kotadia et al., 2014; Zhang and Tu, 2014; Cheng et al., 2017). For instance, the adding of Indium has increased the toughness of SAC solder (Lejuste et al., 2013). For more material related improvement summary detail are shown in Section 2.6.3.

## **2.4 Solder joint fracture analysis**

Fracture mechanics is an approach in analysing failure of a device or structure of matter by measuring the stress in the vicinity of a crack tip against the crack length. It is

used in solid mechanics to calculate the driving force on a crack and then to measure the resistance to fracture. Fracture mechanics apply the physics of stress and strain behaviour of materials including elasticity and plasticity theories. It can be divided into two main fields of analysis: linear elastic fracture mechanic (LEFM) and elastic plastic fracture mechanic (EPFM).

Usually brittle materials (such as alloy) involve LEFM while ductile or soft material like pure metal experience EPFM. In the system where the global stress-strain response of the body is linear and elastic (LEFM), the elastic energy release rate,  $G$ , and the stress intensity factor  $K$  can be used for characterizing cracks in structures. In the elastic-plastic region (EPFM) also called yielding fracture mechanics (YFM), the fracture characterizing parameters are the  $J$ -integral and the crack-tip-opening displacement, CTOD. Under LEFM assumptions, the magnitude of stress at the crack tip is theoretically infinite. However, it is obvious that every material has a finite strength and, as a result, there will always be a small damaged zone around the crack tip. For metals, this damaged zone is referred to as the crack tip plastic zone, the spread of the damage zone compared to the size call the  $K$ -dominant region. The small region around the crack tip for which the states of stress, strain, and displacement are determined by the singular term. If the size of the damaged zone is small enough that it is contained within the  $K$ -dominant region, it may conclude that the similitude condition exists. Hence, different cracks with equal stress intensity factors will have equal damaged zones and behave similar to each other. (LEFM applies when the non-linear deformation of the material is confined to a small region near the crack tip.) However, if this zone is larger than the  $K$ -dominant region (such as in plastic) then the linear elastic assumptions are

not correct, LEFM is not applicable and a nonlinear model (EPFM) is proposed to analyse the relatively large plastic zones.

It has two approaches to quantify the fracture toughness of a material, that is energy criterion and the stress intensity approach. In energy approach, the fracture toughness parameter is the energy release rate ( $G$ ) while in stress intensity approach, the parameter is stress intensity factor ( $K$ ).

#### 2.4.1 Energy release rate ( $G$ ) analysis approach

Energy approach to measure fracture toughness of matter is the earliest method proposed by Irwin in 1956 which equivalent to Griffith model (1920), the founder of Fracture mechanics. The energy approach states that crack extension (i.e., fracture) occurs when the energy available for crack growth is sufficient to overcome the resistance of the material. The material resistance may include the surface energy, plastic work, or other types of energy dissipation associated with a propagating crack. The energy release rate  $G$  which is also defined as the rate of change in potential energy with the crack area for a linear elastic material. At the moment of fracture  $G = G_c$ , the critical energy release rate, which is a measure of fracture toughness. For a crack of length  $2a$  in an infinite plate subject to a remote tensile stress, the energy release rate is given by

Equation (2.1)

$$G = \frac{\pi \sigma^2 a}{E} \quad (2.1)$$

where  $E$  is Young's modulus,  $\sigma$  is the remotely applied stress, and  $a$  is the half-crack length.

#### 2.4.2 $J$ -integral ( $J$ ) analysis approach

Later, further development in fracture parameter and finally come to  $J$  contour integral approach which introduced by  $J.$  Rice especially for non-linear elastic materials.  $J$ -integral is energy approach and in LEFM,  $J = G$ . When  $J$ -integral apply in EPFM,

$$J = \int_{\Gamma} (w dy - T_i \frac{\partial u_i}{\partial x} ds) \quad (2.2)$$

where  $w = \int_0^{\varepsilon_{ij}} \sigma_{ij} d\varepsilon_{ij}$  = strain energy density,  $T_i$  = components of traction vector,  $u_i$  = displacement vector components and  $ds$  = length increment along the contour  $\Gamma$ .  $\Gamma$  is the path around the crack tip,  $\sigma_{ij}$  = stress and  $\varepsilon_{ij}$  = strain tensor. Figure 2.7 describes the random  $J$  contour at the crack tip of a crack.

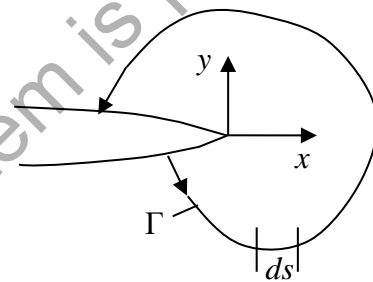


Figure 2.7 Arbitrary contour around the crack tip of a crack. (Anderson, 2005)